

Article

Ex-LDH-Based Catalysts for CO₂ Conversion to Methanol and Dimethyl Ether

Mauro Mureddu ¹, Sarah Lai ¹, Luciano Atzori ², Elisabetta Rombi ², Francesca Ferrara ¹, Alberto Pettinau ¹
and Maria Giorgia Cutrufello ^{2,*}

¹ Sotacarbo S.p.A.—Grande Miniera di Serbariu, SS 126, 09013 Carbonia, Italy; mauro.mureddu@sotacarbo.it (M.M.); sarah.lai@sotacarbo.it (S.L.); francesca.ferrara@sotacarbo.it (F.F.); alberto.pettinau@sotacarbo.it (A.P.)

² Department of Chemical and Geological Sciences, University of Cagliari, 09042 Monserrato, Italy; lucianoatzori@hotmail.it (L.A.); rombi@unica.it (E.R.)

* Correspondence: gcutrufe@unica.it; Tel.: +39-0706754386

Abstract: CO₂-derived methanol and dimethyl ether can play a very important role as fuels, energy carriers, and bulk chemicals. Methanol production from CO₂ and renewable hydrogen is considered to be one of the most promising pathways to alleviate global warming. In turn, methanol could be subsequently dehydrated into DME; alternatively, one-step CO₂ conversion to DME can be obtained by hydrogenation on bifunctional catalysts. In this light, four oxide catalysts with the same Cu and Zn content (Cu/Zn molar ratio = 2) were synthesized by calcining the corresponding CuZnAl LDH systems modified with Zr and/or Ce. The fresh ex-LDH catalysts were characterized in terms of composition, texture, structure, surface acidity and basicity, and reducibility. Structural and acid–base properties were also studied on H₂-treated samples, on which specific metal surface area and dispersion of metallic Cu were determined as well. After in situ H₂ treatment, the ex-LDH systems were tested as catalysts for the hydrogenation of CO₂ to methanol at 250 °C and 3.0 MPa. In the same experimental conditions, CO₂ conversion into dimethyl ether was studied on bifunctional catalysts obtained by physically mixing the ex-LDH hydrogenation catalysts with acid ferrierite or ZSM-5 zeolites. For both processes, the effect of the Al/Zr/Ce ratio on the products distribution was investigated.

Keywords: CO₂ hydrogenation; methanol synthesis; DME synthesis; ex-LDH; bifunctional catalysts



Citation: Mureddu, M.; Lai, S.; Atzori, L.; Rombi, E.; Ferrara, F.; Pettinau, A.; Cutrufello, M.G. Ex-LDH-Based Catalysts for CO₂ Conversion to Methanol and Dimethyl Ether. *Catalysts* **2021**, *11*, 615. <https://doi.org/10.3390/catal11050615>

Academic Editors: Anastasia Macario and Sudip Chakraborty

Received: 23 April 2021

Accepted: 8 May 2021

Published: 11 May 2021

Publisher's Note: MDPI stays neutral with regard to jurisdictional claims in published maps and institutional affiliations.



Copyright: © 2021 by the authors. Licensee MDPI, Basel, Switzerland. This article is an open access article distributed under the terms and conditions of the Creative Commons Attribution (CC BY) license (<https://creativecommons.org/licenses/by/4.0/>).

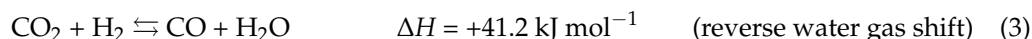
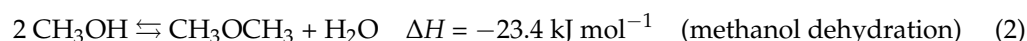
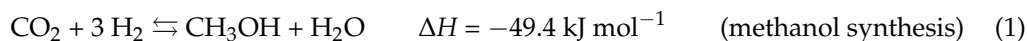
1. Introduction

Clean fuel production from carbon dioxide and the excess of renewable electricity is attracting the interest of the scientific and industrial community [1] since it allows for solving two problems at the same time: first of all, it allows for storing the overproduction of electricity in chemical form [2], with the subsequent stabilization of the electrical grid, and promoting a further exploitation of renewable sources [3]; in parallel, it uses carbon dioxide as a feedstock, generating a circular economy based on carbon, seen as a resource instead of a problem [4,5]. This approach is not limited to the power generation sector, but can also be applied to several kinds of industrial plants (steel and cement in particular) [6].

In this scenario, CO₂-derived methanol and dimethyl ether (DME) can play a very important role as e-fuels (commonly defined as fuels produced using renewable energy), energy carriers, and building blocks in the chemical industry [7].

Methanol is commonly produced from syngas using commercial CuO/ZnO/Al₂O₃ catalysts [8]. However, its production from CO₂ and renewable hydrogen is now considered as one of the most promising pathways to alleviate the global warming and result in production of renewable fuels and valuable chemicals [9].

DME can be synthesized from CO₂ via two sequential steps: catalytic hydrogenation of CO₂ to methanol and methanol dehydration to DME. However, the severe limitations of thermodynamic equilibrium in methanol synthesis are the bottleneck of this process. To overcome this drawback, the one-step hydrogenation of CO₂ to DME over a bifunctional catalyst can be considered as a near-term perspective process. In the synthesis of DME from CO₂, three main reactions take place:



Catalysts for the direct CO₂-to-DME process should be able to efficiently catalyze both methanol synthesis and methanol dehydration reactions, while the yield to CO, formed via the reverse water gas shift side reaction, should be kept to a minimum.

Besides the conventional CuO/ZnO/Al₂O₃, different Cu-based catalytic systems have been investigated for the methanol synthesis from CO₂ [10–13]. Among them, the ZrO₂-containing catalysts have been recently claimed to be very active and selective due to the versatile properties and weak hydrophilic character of zirconia [12].

On the other hand, methanol dehydration reaction takes place rapidly over a solid acid component. Thus, due to the high activity and easy preparation of the Cu-ZnO-based systems, bifunctional catalysts for directly converting CO₂ into DME can be obtained by combining such redox systems with solid acid catalysts [14], among which H-ZSM-5 [8,15–22], ferrierite [17,19,20,23,24], mordenite [17,19,20], and γ -Al₂O₃ [25,26].

Particle size, surface area, metallic Cu⁰ surface area, and composition of the catalyst are important factors that affect catalytic performance; in turn, they are influenced by the catalyst synthesis method. Preparation methods usually involve the co-precipitation of the metal precursors from the liquid phase through sodium carbonate and the subsequent aging step for the formation of crystalline hydroxycarbonate precursors [27,28]. By using a well-controlled co-precipitation method, a Cu/Zn/Al/Zr catalytic system with excellent performance for CO₂ hydrogenation to methanol can be obtained [29,30]. As a result, considerable attention has been recently paid to hydrotalcite-like compounds as catalyst precursors with the general formula of [M²⁺_{1-x}M³⁺_x(OH)₂]^{x+}(Aⁿ⁻)_{x/n}·mH₂O. Such layered double hydroxide (LDH) materials are characterized by a homogeneous dispersion of metal cations at an atomic level, high stability against sintering, high specific surface area, and appropriate basic properties [31,32]. However, to the best of the authors' knowledge, very few papers dealing with the use of redox catalysts obtained by calcination of LDH systems (ex-LDH) for the CO₂ hydrogenation to dimethyl ether have been published so far. This ex-LDH system is peculiar, probably associated to the coordination requirements of Cu²⁺ to form distorted octahedra, introducing the Jahn–Teller effect into the layers and, thereby, destabilizing the hydrotalcite-like structure [30,33]. Therefore, this work aims to probe the ex-LDH compounds for the preparation of ternary and multicomponent redox catalysts for the methanol synthesis and the physical mixture with different acidic catalysts for the CO₂ hydrogenation to dimethyl ether.

2. Results and Discussion

2.1. Characterization of As-Prepared Ex-LDH Catalysts

The chemical composition of the mixed oxides obtained by calcination of the LDH systems is reported in Table 1, in terms of both metal molar ratios and weight percentages of the oxides. It can be observed that the experimental values of the molar ratios are comparable with the nominal ones for all the catalysts and that the CuZnAl sample shows a notably higher amount of copper oxide.

Table 1. Chemical composition of the as-prepared ex-LDH catalysts determined by ICP-AES.

Sample	Molar Ratio Cu/Zn/Al/Zr/Ce	Composition (wt%)				
		CuO	ZnO	Al ₂ O ₃	ZrO ₂	CeO ₂
CuZnAl	2.1/1.0/0.98 (nominal: 2/1/1)	56	27	17	-	-
CuZnAlZr	2.0/1.0/0.80/0.24 (nominal: 2/1/0.7/0.3)	51	26	13	10	-
CuZnAlCe	2.0/1.0/0.76/0.31 (nominal: 2/1/0.7/0.3)	48	24	12	-	16
CuZnAlZrCe	2.0/1.0/0.76/0.13/0.16 (nominal: 2/1/0.7/0.15/0.15)	49	25	12	5	9

The N₂ adsorption/desorption isotherms of the as-prepared ex-LDH samples are shown in Figure 1. All curves are of type IIb, typical for non-porous or macroporous materials, that allow unrestricted multilayer formation at high p/p_0 values [34]. The presence of narrow hysteresis loops is ascribable to the inter-particle capillary condensation. Specific surface areas (S_{BET}) and specific pore volumes (V_p) are summarized in Table 2. Such values are comparable to those obtained for Cu/Zn-based catalysts synthesized by the urea-nitrate combustion method [35], by co-precipitation [36], or from hydrotalcite-like precursors [37–39].

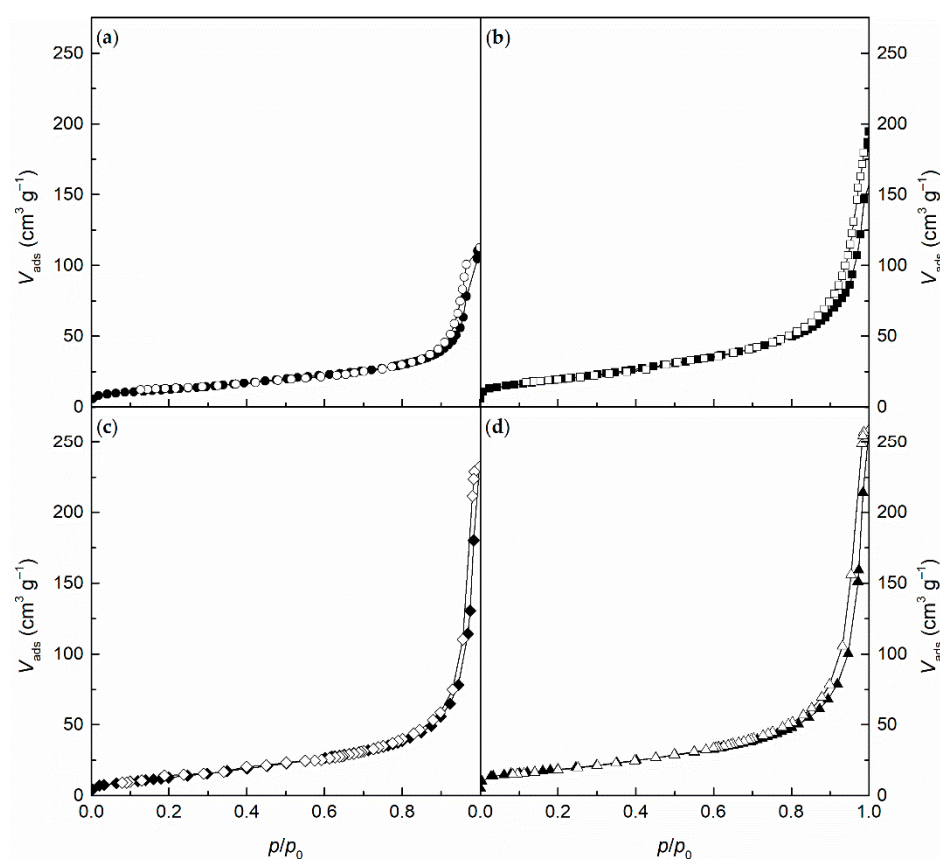
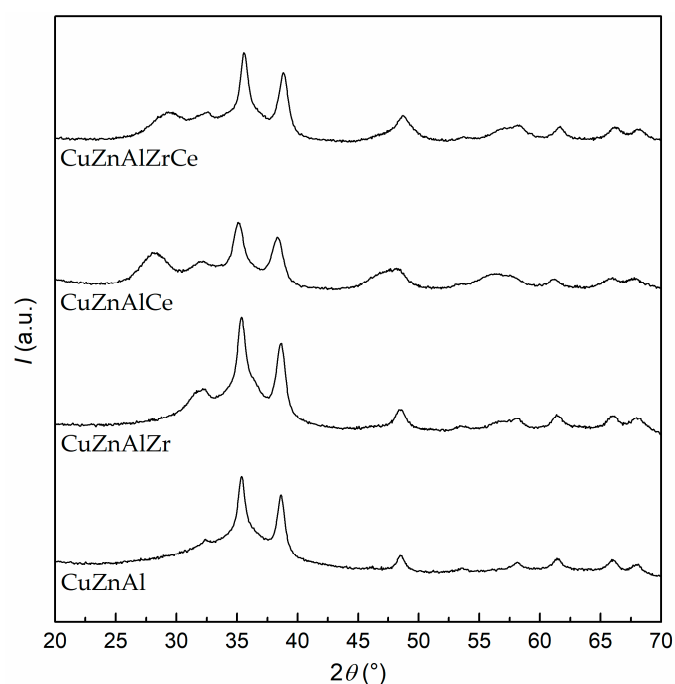
**Figure 1.** N₂ adsorption (full symbols)/desorption (open symbols) isotherms of the as-prepared ex-LDH catalysts: (a) CuZnAl; (b) CuZnAlZr; (c) CuZnAlCe; (d) CuZnAlZrCe.

Table 2. Textural features of the as-prepared ex-LDH catalysts.

Sample	S_{BET} ($\text{m}^2 \text{g}^{-1}$)	V_{p} ($\text{cm}^3 \text{g}^{-1}$)
CuZnAl	45	0.17
CuZnAlZr	64	0.38
CuZnAlCe	49	0.39
CuZnAlZrCe	66	0.41

The X-ray diffraction patterns of the as-prepared ex-LDH mixed oxides are reported in Figure 2. For all the samples, the most definite signals (in particular, the reflections at $2\theta = 35.5^\circ$ and 38.7°) are ascribable to the CuO phase (PDF card 80-1917) and are clearly superimposed to wider signals, related to amorphous or highly dispersed aluminum, zinc, cerium and/or zirconium oxides. Due to such superimposition, the crystallite size calculated by the Scherrer equation in the 8–12 nm range can only be considered as a rough estimate. For CuZnAlCe, wide signals ascribable to nanocrystalline (crystallite size ca. 3 nm) cubic CeO₂ are noticeable at $2\theta = 28.5^\circ$ and 47.5° (PDF card 75-151). For CuZnAlZrCe similar signals are present, but they are shifted to higher angles, most likely due to the formation of a CeO₂-ZrO₂ solid solution.

**Figure 2.** XRD patterns of the as-prepared ex-LDH catalysts.

The surface acidity and basicity of the ex-LDH mixed oxides were investigated by adsorption microcalorimetry of NH₃ and CO₂, respectively. From the combination of the data of the adsorption isotherm (quantity adsorbed as a function of pressure) and of the calorimetric isotherm (integral heat of adsorption as a function of pressure), the curves of the differential heat of adsorption (Q_{diff}) as a function of the amount of adsorbing sites (n) can be obtained, from which it is possible to get information both on the concentration of the sites and on their strength. The results are shown in Figures S1 and S2 and summarized in Table 3. Q_{diff} values of 60 and 40 kJ mol^{-1} , corresponding to about three times the NH₃ and CO₂ condensation heats at 80 °C (20.2 and 13.7 kJ mol^{-1} , respectively), have been considered as the threshold values between chemical and physical or non-specific adsorption: sites with lower adsorption heats have hence been neglected when assessing the acid–base properties of the surface. Thus, the total amount of acid and base sites was obtained ($n_{\text{A,tot}}$: $Q_{\text{diff}} \geq 60 \text{ kJ mol}^{-1}$; $n_{\text{B,tot}}$: $Q_{\text{diff}} \geq 40 \text{ kJ mol}^{-1}$), whereas the strength

distribution of the sites was evaluated by roughly ranking the sites as strong ($n_{A,s}$, $n_{B,s}$: $Q_{diff} \geq 150 \text{ kJ mol}^{-1}$), medium ($n_{A,m}$, $n_{B,m}$: $100 \leq Q_{diff} < 150 \text{ kJ mol}^{-1}$), and weak ($n_{A,w}$: $60 \leq Q_{diff} < 100 \text{ kJ mol}^{-1}$; $n_{B,w}$: $40 \leq Q_{diff} < 100 \text{ kJ mol}^{-1}$) (Table 3).

For all the as-prepared mixed oxides, the differential heat of adsorption of ammonia continuously decreases as the amount adsorbed increases (Figure S1), indicating the presence of energetically heterogeneous acid sites. The existence of a small amount of very strong acid sites can also be inferred from the extremely high initial values of Q_{diff} ($>300 \text{ kJ mol}^{-1}$). After addition of the fourth component to the CuZnAl mixed oxide, a manifest increase in the number of weak acid sites is observed, which is more pronounced in the case of the CuZnAlCe sample. The simultaneous presence of Zr and Ce, together with the increase in the amount of weak acid sites, also determines an increase in the number of the strong sites at the expense of the medium strength ones (Table 3).

Concerning basicity, a very fast decrease in the differential heat of adsorption is visible for all the samples, with values corresponding to physical adsorption that are reached at very low CO_2 adsorbed amount (Figure S2). Despite the high initial value of Q_{diff} , which indicates the presence of an exiguous number of strong sites, the CuZnAl sample has a total amount of basic sites that is one order of magnitude lower than for the other samples in the series (Table 3). However, although remaining fairly limited, the surface basic properties are positively affected by the addition of ZrO_2 and/or CeO_2 , as demonstrated by the increase in the number of medium and weak sites.

Table 3. Acid and base sites strength distribution for the as-prepared ex-LDH catalysts.

Sample	n_A ($\mu\text{mol g}^{-1}$)				n_B ($\mu\text{mol g}^{-1}$)			
	$n_{A,w}$ (a)	$n_{A,m}$ (b)	$n_{A,s}$ (c)	$n_{A,tot}$ (d)	$n_{B,w}$ (e)	$n_{B,m}$ (f)	$n_{B,s}$ (g)	$n_{B,tot}$ (h)
CuZnAl	23	15	15	53	0.2	0.2	1.8	2.2
CuZnAlZr	38	13	19	70	10	6	-	16
CuZnAlCe	47	17	20	84	19	10	-	29
CuZnAlZrCe	47	6	33	86	16	9	-	25

(a) $60 \leq Q_{diff} < 100 \text{ kJ mol}^{-1}$; (b) $100 \leq Q_{diff} < 150 \text{ kJ mol}^{-1}$; (c) $Q_{diff} \geq 150 \text{ kJ mol}^{-1}$; (d) $Q_{diff} \geq 60 \text{ kJ mol}^{-1}$. (e) $40 \leq Q_{diff} < 100 \text{ kJ mol}^{-1}$; (f) $100 \leq Q_{diff} < 150 \text{ kJ mol}^{-1}$; (g) $Q_{diff} \geq 150 \text{ kJ mol}^{-1}$; (h) $Q_{diff} \geq 40 \text{ kJ mol}^{-1}$.

To investigate the reducibility of the oxide catalysts, H_2 temperature programmed reduction analyses were carried out, and the obtained results are shown in Figure 3. As can be seen, the TPR profiles are quite complex and indicate the presence of different reducible species. According to the literature, ZnO [40], Al_2O_3 [41], and ZrO_2 [42] do not undergo reduction processes in the adopted operating conditions. Therefore, the reducible species are reasonably constituted by different copper species, such as highly dispersed and bulk-like CuO phases, whose reducibility might also be affected by the interactions with the other component oxides. However, in the case of the CuZnAlCe and CuZnAlZrCe samples, a minor contribution ascribable to the surface reduction process of ceria at temperatures higher than $300 \text{ }^\circ\text{C}$ cannot be excluded [43]. The TPR curve of CuZnAl shows three distinct peaks of hydrogen consumption, with maxima between 260 and $325 \text{ }^\circ\text{C}$; such a sample appears to be the most difficult to reduce, as its reduction process starts around $170 \text{ }^\circ\text{C}$ (T_{onset}) and is complete at $350 \text{ }^\circ\text{C}$. The addition of ZrO_2 and/or CeO_2 seems to positively influence the reducibility of the CuO species, as indicated by the decrease in T_{onset} ($<150 \text{ }^\circ\text{C}$) and in the temperatures of maximum hydrogen consumption (in the range 210 – $260 \text{ }^\circ\text{C}$). These results are in agreement with those reported in the literature [44], where a shift of the reduction peaks towards higher temperatures was observed after addition of alumina to a CuO - ZnO reference sample and ascribed to the strong interactions between Al_2O_3 and CuO ; conversely, the further addition of ZrO_2 to the catalyst formulation was found to promote the reducibility of the copper oxide phase. The reduction extent for the samples, calculated by determining the amount of H_2 consumed in the reduction process from the area under the TPR curve and considering a $\text{Cu}^{2+}:\text{H}_2$ stoichiometry of 1:1, was found to be $\geq 90\%$, the lowest value being obtained for the CuZnAl sample.

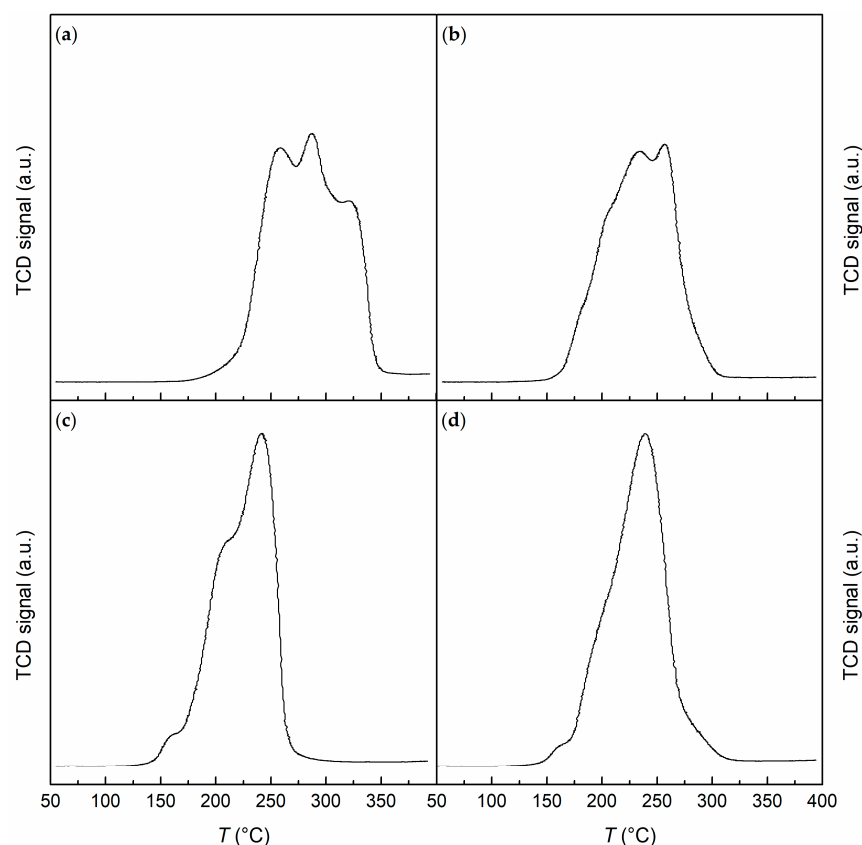


Figure 3. H_2 -TPR profiles of the as-prepared ex-LDH catalysts: (a) CuZnAl; (b) CuZnAlZr; (c) CuZnAlCe; (d) CuZnAlZrCe.

2.2. Characterization of the H_2 -Treated Ex-LDH Catalysts

In order to investigate the effect of the H_2 treatment typically undergone by the catalysts prior to the catalytic tests, the ex-LDH mixed oxides were treated in H_2 atmosphere at 250 °C and characterized.

The XRD patterns of the H_2 -treated ex-LDH samples are reported in Figure 4. For all the samples, besides the same wide signals already observed for the calcined samples (cf. Figure 2), reflections at $2\theta = 43.3^\circ$ and 50.4° are present. The latter are ascribable to metallic copper (PDF card 4-836), which clearly derives from the reduction of CuO, whose signals are no more visible. Metallic copper crystallite size, calculated by the Scherrer equation, is in the range 10–13 nm.

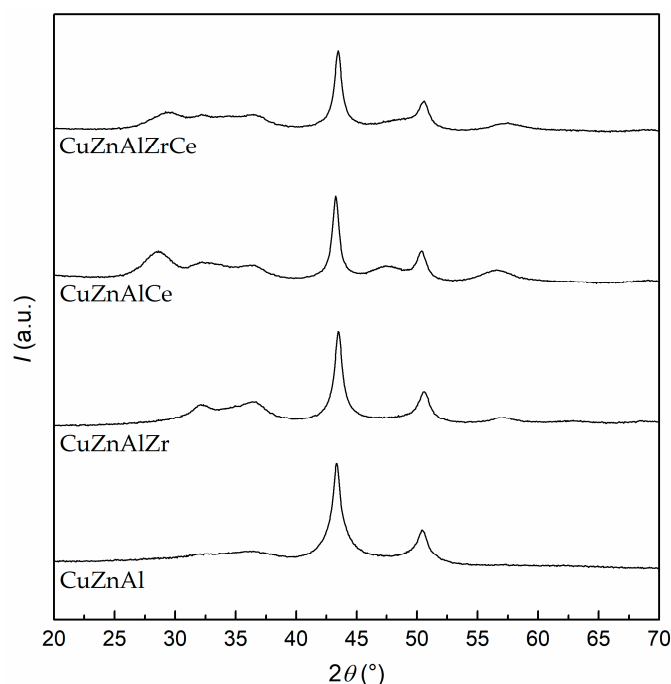


Figure 4. XRD patterns of the H₂-treated ex-LDH catalysts.

The values of the dispersion of metallic Cu (D_{Cu^0}) and of the metallic Cu surface area per mass of catalyst ($A_{Cu^0}^{cat}$) are shown in Table 4. The obtained values indicate a slightly higher copper dispersion in the CuZnAlCe and CuZnAlZrCe samples, possibly due to a lower copper content (wt%) owing to the replacement of Al₂O₃ and/or ZrO₂ with the heavier CeO₂.

Table 4. Dispersion of metallic copper and specific surface area determined on the H₂-treated ex-LDH catalysts by N₂O adsorptive decomposition at controlled temperature followed by H₂-TPR.

Sample	Cu Content ^(a) (wt%)	D_{Cu^0} (%)	$A_{Cu^0}^{cat}$ (m ² g ⁻¹)
CuZnAl	45	6.4	19
CuZnAlZr	41	6.8	18
CuZnAlCe	38	8.1	20
CuZnAlZrCe	39	8.0	20

^(a) Calculated from ICP-AES results (cf. Table 1).

The adsorption microcalorimetry data of the H₂-treated samples are shown in Figures S1 and S2. The curves of Q_{diff} vs. the NH₃ adsorbed amount still present a continuous decrease, confirming the heterogeneity of the surface acid sites from the energetic point of view (Figure S1). It can be noted that, though significantly lower than for the as-prepared samples, the initial values of Q_{diff} for the H₂-treated ones are still higher than 150 kJ mol⁻¹, suggesting that a small number of strong acid sites are still present. By looking at data reported in Table 5, it can be seen that the H₂ treatment leads to an increase in the total number of acid sites, principally due to the increase in the number of weak sites. However, by calculating the fraction of medium and strong sites with respect to the total ones, a general decrease in the acid properties upon H₂ treatment can be highlighted; in fact, these sites together account for percentages in the range 44–57% for the as-prepared oxides, which decrease to values between 29% and 38% for the samples subjected to the H₂ treatment (Table S1).

By looking at the curves of Q_{diff} as a function of CO₂ adsorbed amount (Figure S2), it can be noted that the initial values of Q_{diff} are significantly higher than those of the as-prepared oxides, except for the CuZnAl sample. In addition, all the curves of the H₂-

treated samples lie above those of the as-prepared ones, suggesting an increase in the basic surface properties. For the CuZnAlCe sample, the presence of a family of homogeneous weak base sites is also revealed by a well-defined plateau observable at ca. 70 kJ mol⁻¹. Interestingly, the increase in basicity is largely due to the increase in the number of strong sites (Table 5). Except for CuZnAl (which shows a much lower amount of basic sites than the other samples in the series), the percentages of medium and strong sites increase in comparison with those of the as-prepared oxides, confirming their higher basicity after the H₂ treatment.

Notably, by comparing the acidic and basic properties of the reduced catalysts, it appears that, for CuZnAl, the number of total acid sites is more than ten times greater than that of the basic ones. In the case of the other catalysts, the value of the $n_{A,tot}/n_{B,tot}$ ratio is much lower, being in the order CuZnAlZr > CuZnAlZrCe > CuZnAlCe (Table S1). In addition, in the case of the Zr- and/or Ce-containing samples also the value of $n_{A,(m+s)}/n_{B,(m+s)}$ is significantly lower than that of CuZnAl and is the lowest for the CuZnAlCe, pointing out the former as the most acidic catalyst and the latter as the most basic one.

Table 5. Acid and base sites strength distribution for the H₂-treated LDH samples.

Sample	n_A ($\mu\text{mol g}^{-1}$)				n_B ($\mu\text{mol g}^{-1}$)			
	$n_{A,w}$ ^(a)	$n_{A,m}$ ^(b)	$n_{A,s}$ ^(c)	$n_{A,tot}$ ^(d)	$n_{B,w}$ ^(e)	$n_{B,m}$ ^(f)	$n_{B,s}$ ^(g)	$n_{B,tot}$ ^(h)
CuZnAl	53	17	12	82	3	1	3	7
CuZnAlZr	67	23	19	109	18	3	8	29
CuZnAlCe	102	29	12	143	20	13	16	49
CuZnAlZrCe	72	20	17	109	14	6	14	34

^(a) $60 \leq Q_{diff} < 100$ kJ mol⁻¹; ^(b) $100 \leq Q_{diff} < 150$ kJ mol⁻¹; ^(c) $Q_{diff} \geq 150$ kJ mol⁻¹; ^(d) $Q_{diff} \geq 60$ kJ mol⁻¹. ^(e) $40 \leq Q_{diff} < 100$ kJ mol⁻¹; ^(f) $100 \leq Q_{diff} < 150$ kJ mol⁻¹; ^(g) $Q_{diff} \geq 150$ kJ mol⁻¹; ^(h) $Q_{diff} \geq 40$ kJ mol⁻¹.

2.3. Characterization of the Zeolite Catalysts

The bifunctional catalysts used for DME synthesis were obtained by physically mixing the ex-LHD oxides with three acid zeolites (obtained by calcining the commercial ammonium form): one ferrierite with SiO₂/Al₂O₃ ratio of 20:1 (FER_20) and two ZSM-5, with SiO₂/Al₂O₃ molar ratios of 350:1 and 23:1 (ZSM5_350 and ZSM5_23, respectively). The surface acidity of the zeolite samples was investigated by adsorption microcalorimetry of ammonia and the curves of Q_{diff} as a function of the adsorbed amount of NH₃ are shown in Figure 5. After a very high initial value (> 275 kJ mol⁻¹), indicative of the presence of a low number of very strong acid sites, the adsorption heat decreases at increasing NH₃ adsorbed amount. Such a decrease is particularly fast for the ZSM5_350 sample, for which heat values typical for non-specific adsorption are achieved at extremely low ammonia adsorption. In the case of FER_20 and ZSM5_23 a quasi-plateau is observable in the range 100–150 kJ mol⁻¹, which is more evident for the former catalyst and suggests the existence of energetically homogeneous sites.

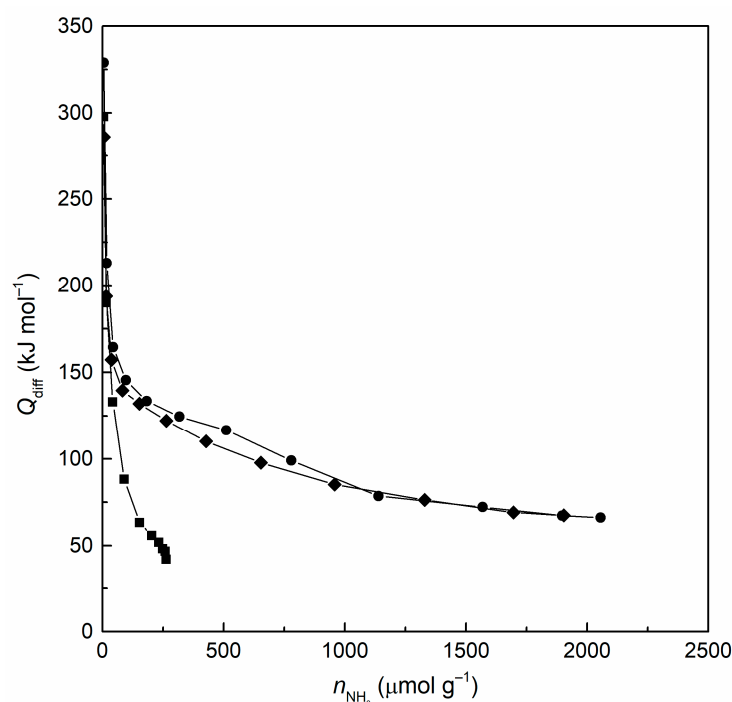


Figure 5. Differential heat of adsorption of NH_3 as a function of the amount of the adsorbing sites for zeolite samples: (●), FER_20; (◆), ZSM5_23; (■), ZSM5_350.

The surface acid properties are summarized in Table 6 in terms of sites strength distribution. FER_20 and ZSM5_23 show similar acid properties, both in terms of sites concentration and strength distribution, while the ZSM5_350 sample possesses a number of sites that is one order of magnitude lower than for the other two samples. This result, as well as the remarkable increase in the fraction of strong acid sites (Table 6), is expected as a consequence of dealumination.

Table 6. Acid sites strength distribution for the zeolite samples.

Sample	n_A ($\mu\text{mol g}^{-1}$)			n_A Distribution (%)			
	$n_{A,w}$ (a)	$n_{A,m}$ (b)	$n_{A,s}$ (c)	$n_{A,tot}$ (d)	$n_{A,w}/n_{A,tot}$	$n_{A,m}/n_{A,tot}$	$n_{A,s}/n_{A,tot}$
FER_20	1292	681	83	2056	63	33	4
ZSM5_23	1293	555	56	1904	68	29	3
ZSM_350	96	45	33	174	55	26	19

(a) $60 \leq Q_{diff} < 100 \text{ kJ mol}^{-1}$; (b) $100 \leq Q_{diff} < 150 \text{ kJ mol}^{-1}$; (c) $Q_{diff} \geq 150 \text{ kJ mol}^{-1}$; (d) $Q_{diff} \geq 60 \text{ kJ mol}^{-1}$.

2.4. Catalytic Results for CO_2 Conversion to Methanol

The ex-LDH oxide samples were tested as catalysts for the CO_2 hydrogenation to methanol in 24-h runs. CO_2 conversion (X_{CO_2}) as a function of time on stream are reported in Figure S3. Very similar and almost constant X_{CO_2} values were obtained for all samples with the exception of CuZnAlCe, for which conversion is somewhat lower and slightly decreasing with time on stream. Average values (over 24 h on stream) of CO_2 conversion (X_{CO_2}), selectivity to different products (S_i), as well as methanol yield ($Y_{\text{CH}_3\text{OH}}$) and space time yield ($STY_{\text{CH}_3\text{OH}}$), are reported in Table 7 and Figure S4. Under the conditions of the catalytic tests, the main products of CO_2 hydrogenation were methanol and carbon monoxide, water being coproduced in both reactions. Light hydrocarbons (methane, ethane, and propane) were also monitored during the reaction and detected in very low amounts.

Table 7. Catalytic results (average values over 24 h on stream) for CO₂ hydrogenation to methanol on ex-LDH oxides. Reaction conditions: $T = 250\text{ }^{\circ}\text{C}$; $P = 3.0\text{ MPa}$; $\text{H}_2/\text{CO}_2 = 3\text{ mol mol}^{-1}$; $\text{GHSV} = 12,000\text{ Ncm}^3\text{ g}_{\text{cat}}^{-1}\text{ h}^{-1}$.

Catalyst	X_{CO_2} (mol%)	S_{CO} (mol%)	$S_{\text{CH}_3\text{OH}}$ (mol%)	S_{DME} (mol%)	$S_{\text{C}_n\text{H}_{(2n+2)}}$ (mol%)	$Y_{\text{CH}_3\text{OH}}$ (mol%)	$STY_{\text{CH}_3\text{OH}}$ ($\text{mg}_{\text{CH}_3\text{OH}}/\text{g}_{\text{cat}}\text{ h}^{-1}$)
CuZnAl	18.6	65.3	27.7	6.9	0.1	5.2	205
CuZnAlZr	18.7	66.3	33.7	traces	traces	6.3	250
CuZnAlCe	14.2	61.6	37.8	0.6	traces	5.4	213
CuZnAlZrCe	17.9	64.7	32.5	2.6	0.2	5.8	230

The non-negligible value of the DME selectivity for the CuZnAl catalyst can be reasonably explained by considering its surface acid–base properties, which highlight the definite predominance of acidic sites compared to basic ones (cf. Table 5 and Table S1).

As expected, the catalytic performance is affected by the presence of zirconium and/or cerium. The partial substitution of aluminum with zirconium in the CuZnAlZr catalyst, while retaining the same conversion of the CuZnAl catalyst despite the lower Cu content, enhances the selectivity to methanol at the expense of the formed amount of DME, thus leading to a manifest increase in the productivity of methanol (Table 7). Though the synergistic effects induced by ZrO₂ have been extensively investigated, its multiple roles in the catalytic process are still under debate. ZrO₂ is known to enhance the Cu/Zn dispersion and the redox properties of the Cu species [12]. In the present case, the positive effect of Zr addition on the textural properties of CuZnAlZr in comparison with CuZnAl is proved by the increase in the S_{BET} and V_{p} values (cf. Table 2); conversely, no appreciable differences are observed between the two catalysts with regard to dispersion and specific surface area of Cu (cf. Table 4). Thus, the improvement of the catalytic performance in terms of $STY_{\text{CH}_3\text{OH}}$ is reasonably ascribable to the changes in the acid–base properties, in that the decrease in DME formation would be due to the remarkable decrease in the $n_{\text{A,tot}}/n_{\text{B,tot}}$ ratio (cf. Table S1). Notably, the present CuZnAlZr catalyst shows better performance than a similar sample (CHT-Al0.9 in [38]), which—despite the higher Cu dispersion and the higher operating pressure—presented a lower space time yield ($0.19\text{ g}_{\text{CH}_3\text{OH}}\text{ g}_{\text{cat}}^{-1}\text{ h}^{-1}$). In fact, the main difference in the composition of the two systems is the higher Zr content in the present CuZnAlZr sample, which is in line with the already observed beneficial effect of zirconium.

For the CuZnAlCe catalyst, where Zr is completely replaced by cerium, a lower conversion is observed, which is, however, accompanied by a notably higher $S_{\text{CH}_3\text{OH}}$, compared to the CuZnAl catalyst and also to both the Zr-containing samples. In the literature, decreasing trends in CO₂ conversion in the presence of ceria were already observed for Cu–ZnO systems supported on Zr_xCe_(1–x)O₂ ($0 \leq x \leq 1$) [45] or for CuZnMO_x oxides (M = Al, Zr, Ce, Ce–Zr) [46] and were ascribed to its lower efficiency in improving the textural properties and metal surface area of the catalyst in comparison with zirconia. On the other hand, the increase in methanol selectivity was attributed to the promoting effect of ceria in adsorbing and activating the CO₂ molecule. For M-promoted CuZnAl catalysts (M = Mn, La, Ce, Zr, Y), the selectivity to CH₃OH was found to be correlated with the increase in the strength of the surface basic sites, which were classified as weak (α), moderate (β), and strong (γ) ones by temperature programmed desorption of CO₂ [47]. It was proposed that CO₂ is adsorbed on the basic sites in different forms depending on their strength: bicarbonates species, which easily desorb without giving rise to the reactive event, arise from the interaction with the α sites, whereas carbonate intermediates are formed on stronger sites and can be hydrogenated by hydrogen activated on the Cu sites. Formaldehyde was proposed as a common intermediate, which can lead to the formation of CH₃OH or CO depending on whether it is adsorbed on γ or β basic sites, respectively. According to the literature, the enhanced value of CH₃OH selectivity shown by the CuZnAlCe catalyst can hence be explained in light of its higher basic character.

Concerning CO₂ conversion and methanol space–time yield, no significant differences are observed in the $A_{Cu^0}^{cat}$ values between CuZnAlZr and CuZnAlCe (cf. Table 4), although the latter has a lower S_{BET} (cf. Table 2); therefore, the worsening of its catalytic activity might tentatively be explained by an unbalanced ratio between the Cu and the basic sites responsible for the activation of H₂ and CO₂, respectively.

The partial substitution of Zr with Ce in the CuZnAlZrCe catalyst does not improve either CO₂ conversion or methanol selectivity compared to CuZnAlZr; on the contrary it leads to a decrease in the STY_{CH_3OH} value (cf. Table 7). The lack of a synergistic effect might be due to a non-optimal Ce/Zr molar ratio. Indeed, it was observed in the literature [48,49] that the catalytic behavior is positively affected by the simultaneous presence of Ce and Zr for Ce/Zr ratios up to 1 and worsens for higher values.

2.5. Catalytic Results for CO₂ Conversion to Dimethyl Ether

Some fundamental aspects are considered to play a key role for developing catalytic systems with high DME productivity: (i) the stability in the presence of water should be high; (ii) the formation of olefins should be avoided; (iii) the acidic sites should be well distributed and of suitable strength [19,50]. A study on syngas to dimethyl ether conversion using different zeolites (Theta-1, ZSM-23, ferrierite, ZSM-5) in mixture with a commercial Cu/ZnO/Al₂O₃ redox catalyst reported a superior catalytic performance in the presence of ferrierite, which was ascribed to its topology that limits the formation of hydrocarbons owing to a preferential path for the diffusion of small reactants and products [17].

Bifunctional catalysts were then prepared by mixing the acid ferrierite zeolite (FER_20) and the redox ex-LDH synthesized systems and tested for the direct CO₂ hydrogenation to DME. The two components were mixed in a 1:1 weight ratio, since it was reported as the most performing [17,51]. CO₂ conversion (X_{CO_2}) as a function of time on stream (Figure S5) showed that all the catalysts are stable within the investigated reaction time except for the bifunctional system containing CuZnAlCe, which confirms the presence of a slight deactivation, as already observed for such sample during the synthesis of methanol (cf. Figure S3). Table 8 and Figure S6 summarize the catalytic performance in terms of average values (over 24 h on stream) of CO₂ conversion, selectivity to different products (S_i), DME yield (Y_{DME}) and space time yield (STY_{DME}). Under the employed reaction conditions, the only products of the CO₂ hydrogenation are DME, methanol, and carbon monoxide, water being coproduced in all the three reactions. Traces of light hydrocarbons (methane, ethane and propane) were also detected.

Table 8. Catalytic results (average values over 24 h on stream) for CO₂ hydrogenation to DME on ex-LDH/zeolite bifunctional systems. Reaction conditions: $T = 250$ °C; $P = 3.0$ MPa; $H_2/CO_2 = 3$ mol mol⁻¹; $GHSV = 6000$ Ncm³ g_{cat}⁻¹ h⁻¹.

Catalyst	X_{CO_2} (mol%)	S_{CO} (mol%)	S_{CH_3OH} (mol%)	S_{DME} (mol%)	$S_{C_nH_{(2n+2)}}$ (mol%)	Y_{DME} (mol%)	STY_{DME} (mg _{DME} g _{cat} ⁻¹ h ⁻¹)
CuZnAl/FER_20	17.3	61.4	10.5	28.1	-	4.9	139
CuZnAlZr/FER_20	17.0	58.7	9.1	32.0	0.2	5.4	161
CuZnAlCe/FER_20	13.4	63.0	10.6	26.4	traces	3.5	100
CuZnAlZrCe/FER_20	15.8	62.4	9.9	27.6	0.1	4.4	124
CuZnAlZr/ZSM5_23	15.4	59.0	9.1	31.8	0.1	4.9	140
CuZnAlZr/ZSM5_350	18.9	56.9	9.9	33.2	traces	6.3	179

Compared to the results obtained for the methanol synthesis (cf. Table 7) on the corresponding ex-LDH components, a decrease in CO₂ conversion (in the range 6–12%) can be observed for all the catalysts; such a decrease is particularly low for the CuZnAlCe/FER_20 sample, which, however, shows the lowest X_{CO_2} value. Unlike what observed for the corresponding single redox components in the CO₂ hydrogenation reaction, the CO selectivity for the CuZnAlCe/FER_20 bifunctional system is similar to that of CuZnAl/FER_20. Conversely, compared to the results previously obtained with CuZnAlZr,

the CuZnAlZr/FER_20 catalyst shows an evident decrease (ca. 11%) in S_{CO} , also exhibiting the highest values of DME selectivity and yields (Table 8). The superior performance of this bifunctional catalyst is in agreement with the higher methanol productivity formerly shown by the redox CuZnAlZr component (cf. Table 7).

The influence of the different zeolite framework and of the SiO_2/Al_2O_3 molar ratio was also checked. For this purpose, two more bifunctional systems were obtained by mixing the CuZnAlZr sample with two ZSM-5 zeolites having different SiO_2/Al_2O_3 ratios (ZSM5_23 and ZSM5_350). CO_2 conversion (X_{CO_2}) as a function of time on stream, obtained on the two ZSM-5-containing bifunctional systems, is reported in Figure S7, where the results for CuZnAlZr/FER_20 are also reported for comparison. The catalytic behavior of the CuZnAlZr/FER_20 and CuZnAlZr/ZSM5_23 catalysts, where the acidic components have 2-D and 3-D pore channel systems, respectively, but similar SiO_2/Al_2O_3 molar ratios, was compared to verify the effect of the zeolite microstructure. The pertinent results, reported in Table 8 and Figure S8, show that the ZSM-5-containing catalyst performs slightly worse (10% less CO_2 converted) than the one with ferrierite, leading to lower Y_{DME} and STY_{DME} values. Concerning the synthesis of DME from syngas [17] or from methanol in vapor phase [22] using different zeolites (1-D, 2-D, and 3-D channel structures), it was found that the 2-D porous system of ferrierite ensures a high resistance to deactivation by inhibiting the deposition of coke. However, in the present case, no deactivation occurs within the investigated time on stream (Figure S7), the better performance of the CuZnAlZr/FER_20 catalyst being possibly related to its somewhat higher number of medium and strong acid sites.

It is well known that for reactions in which water participates as a reactant or as a product, a drawback in using solid acids is the poisoning of acid sites by water; therefore, the use of water-tolerant catalysts should allow better results in terms of activity and stability. Indeed, due to the hydrophobic character of the surface, which increases with the increase in the Si/Al ratio, high-silica zeolites were found to be very efficient in the case of esterification reactions [52]. In the present case, by comparing the same ZSM-5 structure with different SiO_2/Al_2O_3 molar ratios (Table 8), it appears that the CuZnAlZr/ZSM5_350 catalyst, which contains the high-silica zeolite, shows a better catalytic activity, with Y_{DME} and STY_{DME} values higher by approximately 29% in comparison with CuZnAlZr/ZSM5_23. According to reference [52], this result can be explained taking into account the hydrophobic character of the ZSM5_350 surface, which would favor the adsorption of methanol instead of water, favoring its transformation into DME, provided that the number of the available acid sites is sufficient.

3. Materials and Methods

3.1. Materials

All the chemicals (analytical grade), used as received without any further purification, were purchased from Sigma-Aldrich (St. Louis, Missouri, MI, USA).

3.2. Preparation of Catalysts

3.2.1. Preparation of Hydrogenation Catalysts for Methanol Synthesis

One CuZnAl LDH system and three modifications obtained through incorporation of Zr and/or Ce were prepared at room temperature by co-precipitation at low supersaturation [53]. The samples were synthesized with different Al/Zr/Ce molar ratios, but keeping the value of the Cu/Zn/(Al + Zr + Ce) molar ratio of 2:1:1. For a typical synthesis, two solutions were prepared, the first (100 cm³) containing the desired precursor metal nitrates in appropriate amounts (total cation concentration equal to 1.5 M) and the second obtained by dissolving 13.95 g of NaOH and 7.15 g of Na₂CO₃ in 100 cm³ of distilled water. The two solutions were then mixed under stirring, adjusting the flow rates in order to keep the pH constant (pH = 11). The final suspension was aged under stirring at 60 °C for 20 h and then cooled down to room temperature. The precipitate was filtered off, repeatedly washed

with distilled water, and dried in oven at 80 °C overnight. The LDH systems were finally calcined at 500 °C for 4 h to obtain the corresponding mixed oxide catalysts (ex-LDH).

3.2.2. Preparation of Bifunctional Catalysts for DME Synthesis

Commercial zeolites were used to prepare physical mixtures with the aforementioned ex-LDH redox catalysts. One ferrierite ($\text{SiO}_2/\text{Al}_2\text{O}_3 = 20:1$, surface area = $400 \text{ m}^2 \text{ g}^{-1}$) and two ZSM-5 (with $\text{SiO}_2/\text{Al}_2\text{O}_3$ molar ratios of 23:1 and 350:1 and surface areas of $425 \text{ m}^2 \text{ g}^{-1}$ and $400 \text{ m}^2 \text{ g}^{-1}$, respectively) zeolites were purchased from Alfa Aesar (Kandel, Germany) in the ammonium form. The zeolites were transformed into the protonic form by calcination at 550 °C for 5 h (heating rate, $3 \text{ }^\circ\text{C min}^{-1}$).

3.3. Characterization of Catalysts

The chemical composition of the ex-LDH mixed oxides was determined by inductively coupled plasma atomic emission spectroscopy (ICP-AES). Samples (ca. 0.015 g) were dissolved in 2 cm^3 of a mixture of HCl (37%) and HNO_3 (70%) (3:1 by volume). After 24 h, the solutions were diluted to 250 cm^3 with Milli-Q water and analyzed with a Liberty 200 spectrophotometer (Varian, Palo Alto, California, CA, USA).

Textural analyses were performed on a Sorptomatic 1990 System (Fisons Instrument, Glasgow, UK) by determining the nitrogen adsorption/desorption isotherms at $-196 \text{ }^\circ\text{C}$. Prior to the analysis, the samples were heated overnight under vacuum up to $220 \text{ }^\circ\text{C}$ (heating rate $1 \text{ }^\circ\text{C min}^{-1}$). The Brunauer–Emmett–Teller (BET) specific surface area and the specific pore volume were assessed from the adsorption data [34].

The X-ray diffraction (XRD) analysis was performed on the as-prepared and on the H_2 -treated (5 vol% H_2 in N_2 ; flow rate, $15 \text{ cm}^3 \text{ min}^{-1}$ at $250 \text{ }^\circ\text{C}$ for 2 h) samples. XRD patterns were recorded on a X'pert Pro diffractometer (Panalytical, Malvern, UK) with θ - θ Bragg-Brentano geometry, $\text{Cu-K}\alpha_1$ wavelength radiation ($\lambda = 1.54060 \text{ \AA}$) and X'Celerator detector, operating at 40 kV and 40 mA. The crystallite size was estimated by the Scherrer equation using the Warren correction [54].

Adsorption microcalorimetry measurements were performed with a Tian–Calvet heat flow microcalorimeter (Setaram, Caluire, France), equipped with a volumetric vacuum line. Each sample (0.1 g, 40–80 mesh), as prepared or previously H_2 -treated (5 vol% H_2 in N_2 ; flow rate, $15 \text{ cm}^3 \text{ min}^{-1}$) at $250 \text{ }^\circ\text{C}$ for 2 h, was thermally pretreated at $220 \text{ }^\circ\text{C}$ for 12 h under vacuum ($5 \cdot 10^{-3} \text{ Pa}$). Adsorption was carried out by admitting successive doses of the probe gas (NH_3 or CO_2) at $80 \text{ }^\circ\text{C}$ in order to limit physisorption. The equilibrium pressure relative to each adsorbed amount was measured by means of a differential pressure gauge and the thermal effect was recorded. The run was stopped at a final equilibrium pressure of about 133 Pa.

Temperature-programmed reduction (TPR) profiles were recorded on a TPD/R/O 1100 apparatus (Thermo Fisher Scientific, Waltham, Massachusetts, MA, USA) under the following conditions: sample weight, 0.030 g; heating rate (from 40 to $400 \text{ }^\circ\text{C}$), $10 \text{ }^\circ\text{C min}^{-1}$; flow rate, $30 \text{ cm}^3 \text{ min}^{-1}$; H_2 concentration, 5 vol% in N_2 . Prior to the experiment, samples were pretreated in nitrogen ($20 \text{ cm}^3 \text{ min}^{-1}$) at $350 \text{ }^\circ\text{C}$ for 2 h. The hydrogen consumption was monitored by a thermal conductivity detector (TCD).

The copper dispersion and the specific metal surface area were evaluated by N_2O adsorptive decomposition at controlled temperature (N_2O reacts with metallic Cu on the catalyst surface to form Cu_2O and N_2), followed by H_2 temperature-programmed-reduction of the Cu_2O surface layers formed [55]. Analyses were performed on a TPD/R/O 1100 apparatus (Thermo Fisher Scientific) using the following procedure: ca. 0.1 g of fresh catalyst was first exposed to a H_2/N_2 mixture (H_2 , 5 vol% in N_2 ; flow rate, $15 \text{ cm}^3 \text{ min}^{-1}$) at $250 \text{ }^\circ\text{C}$ for 2 h for reducing copper oxide to metallic copper; then, pulses of N_2O (0.347 cm^3) were admitted to the sample at $40 \text{ }^\circ\text{C}$ using He as the gas carrier ($100 \text{ cm}^3 \text{ min}^{-1}$). The oxidation of the surface metallic copper to Cu(I) was considered complete when the area of the N_2O pulses remained constant, indicating that the reactant was no longer consumed in the reaction. Finally, a H_2 -TPR run (H_2 , 5 vol% in N_2 ; flow rate, $20 \text{ cm}^3 \text{ min}^{-1}$)

was performed from 40° to 400 °C (heating rate, 10 °C min⁻¹). The copper dispersion (D_{Cu^0}) and the Cu specific metal surface area per mass of catalyst ($A_{\text{Cu}^0}^{\text{cat}}$) were calculated by the following equations:

$$D_{\text{Cu}^0} = \frac{n_{\text{H}_2}^{\text{cat}} \times \alpha_{\text{Cu}/\text{H}_2} \times M_{\text{Cu}}}{W_{\text{Cu}}} \times 100 \quad (4)$$

$$A_{\text{Cu}^0}^{\text{cat}} = \frac{n_{\text{H}_2}^{\text{cat}} \times \alpha_{\text{Cu}/\text{H}_2} \times N_{\text{A}}}{\rho_{\text{Cu}^0}^{\text{s}}} \quad (5)$$

where $n_{\text{H}_2}^{\text{cat}}$ is the number of moles of H₂ consumed per mass of catalyst, $\alpha_{\text{Cu}/\text{H}_2}$ is the stoichiometric ratio ($\alpha_{\text{Cu}/\text{H}_2} = \nu_{\text{Cu}}/\nu_{\text{H}_2} = 2 \text{ mol}_{\text{Cu}} \text{ mol}_{\text{H}_2}^{-1}$), M_{Cu} is the copper molar mass, W_{Cu} is the bulk copper content (weight fraction), N_{A} is the Avogadro constant ($6.022 \times 10^{23} \text{ atoms mol}^{-1}$), and $\rho_{\text{Cu}^0}^{\text{s}}$ is the copper surface density ($1.46 \times 10^{19} \text{ atoms m}^{-2}$). Calibration of the H₂ amount consumed was previously carried out by using a copper oxide standard.

3.4. Catalytic Testing

The catalytic activity was investigated in a customized Microactivity Effi (PID Eng&Tech, Madrid, Spain) benchscale plant, employing a high-pressure fixed bed stainless steel reactor (length 304.8 mm, inner diameter 9.1 mm). A porous plate (made of Hastelloy C, 20 μm) and quartz wool were used to support the catalytic bed inside the isothermal temperature zone of the reactor [56,57].

For methanol synthesis experiments, the reactor was loaded with 1.00 g of catalyst, previously diluted with 2.50 g of α-Al₂O₃, in order to obtain a total bed volume of ca. 3 cm³.

DME synthesis tests were performed using a physical mixture obtained combining 1.00 g of the methanol synthesis catalyst and 1.00 g of the one containing the acidic functionality; the obtained bifunctional catalytic system was diluted with 1.00 g of α-Al₂O₃, in order to reach a total bed volume of ca. 3 cm³.

Prior to catalytic tests, all fresh catalysts were reduced in situ in a stream of a H₂/N₂ mixture (H₂, 15 vol% in N₂) at 250 °C for 2 h at atmospheric pressure. Upon completion of the reduction process, the system was maintained at 250 °C, and the reaction gas mixture containing H₂ and CO₂ (molar ratio of 3:1) and 10 vol% of N₂ (used as internal standard for gas chromatographic analysis) was fed. The hydrogenation of CO₂ to methanol and DME was carried out at 3.0 MPa and gas hourly space velocity (GHSV) of 12,000 and 6000 Ncm³ g_{cat}⁻¹ h⁻¹, respectively. After allowing the system to reach the steady state in 1 h on stream, analysis was periodically performed within the 24-hour runs. The reaction stream was analyzed by a 7890B (Agilent, Santa Clara, California, CA, USA) gas chromatograph equipped with a flame ionized detector (FID) for carbon-containing compounds and a thermal conductivity detector (TCD) for permanent gases. Two columns connected in series were used to identify the components of the outlet gas mixture. In particular, CO₂, methanol, dimethyl ether, ethane, and propane were separated by a HP-Plot Q (Agilent) column (length 30 m, inner diameter 0.53 mm, film thickness 40 μm), while a HP-PLOT Molesieve (Agilent) column (length 30 m, inner diameter 0.53 mm, film thickness 50 μm) was used for H₂, N₂, CH₄, and CO. To avoid condensation of condensable products, the connection lines between the plant gas outlet and gas chromatograph inlet were heated at 180 °C. CO₂ conversion (X_{CO_2}), products selectivity (S_{P} , with P: CH₃OH, DME, or CO), and products yield (Y_{P} , with P: CH₃OH or DME), were calculated as follows:

$$X_{\text{CO}_2} = \frac{n_{\text{CO}_2}^{\text{in}} - n_{\text{CO}_2}^{\text{out}}}{n_{\text{CO}_2}^{\text{in}}} \times 100 \quad (6)$$

$$S_{\text{P}} = \frac{\nu_{\text{CO}_2}}{\nu_{\text{P}}} \times \frac{n_{\text{P}}^{\text{out}}}{n_{\text{CO}_2}^{\text{in}} - n_{\text{CO}_2}^{\text{out}}} \times 100 \quad (7)$$

$$Y_P = \frac{\nu_{\text{CO}_2}}{\nu_P} \times \frac{n_P^{\text{out}}}{n_{\text{CO}_2}^{\text{in}}} \times 100 \quad (8)$$

where n_i^{in} and n_i^{out} are the number of moles of the i -th species in the feed or in the gas mixture exiting from the reactor, respectively, and ν_i is the stoichiometric coefficient of the i -th species in the corresponding balanced equation.

The space–time yield of methanol and DME (STY_P , with P: CH₃OH or DME), i.e., the amount of product formed per gram of catalyst per hour ($\text{mg}_P \text{g}_{\text{cat}}^{-1} \text{h}^{-1}$) was determined by the formula:

$$STY_P = \frac{Y_P}{100} \times \frac{\varphi_{\text{CO}_2} \times M_P}{m_{\text{cat}}} \times 1000 \quad (9)$$

where Y is the product yield, φ_{CO_2} is the inlet CO₂ molar flow rate (mol h^{-1}), M_P is the product molar mass (g mol^{-1}), and m_{cat} is the catalyst mass (g). Each catalytic run was performed three times with standard deviations in the range 2–5% for both conversion and selectivity.

4. Conclusions

Four oxide catalysts with the same Cu and Zn content (Cu/Zn = 2 mol/mol) were obtained by calcining the corresponding CuZnAl LDH systems, also modified with Zr and/or Ce. The ex-LDH oxides were tested, after in situ H₂ treatment, as catalysts for the hydrogenation of CO₂ to methanol. The presence of Zr showed a beneficial effect, which could be related to the influence on the acid–base properties, assessed by means of adsorption microcalorimetry. The observation of a positive effect of zirconium was supported by the superior catalytic performance showed by the CuZnAlZr system with respect to a similar catalyst, reported in the literature, characterized by a lower Zr content.

By mixing the CuZnAlZr redox catalyst with a ferrierite zeolite, a good bifunctional system for the one-step CO₂ conversion into DME was also obtained, further confirming the favorable influence of Zr on the catalytic performance. Comparing two catalysts containing ZSM-5 zeolites with different Si/Al ratio revealed that, besides the acid–base properties, the surface hydrophobicity also significantly affects DME formation.

Supplementary Materials: The following are available online at <https://www.mdpi.com/article/10.3390/catal11050615/s1>, Figure S1: Differential heat of adsorption of NH₃ as a function of the amount of adsorbing sites for the ex-LDH samples, Figure S2: Differential heat of adsorption of CO₂ as a function of the amount of adsorbing sites for the ex-LDH samples, Table S1: Percentage of sites of different strength with respect to the total number and n_A/n_B ratios for the mixed oxides catalysts as-prepared and after H₂ treatment, Figure S3: CO₂ conversion as a function of time on stream for the CO₂ hydrogenation to methanol on the ex-LDH catalysts, Figure S4: Catalytic results for CO₂ hydrogenation to methanol on ex-LDH oxides, Figure S5: CO₂ conversion as a function of time on stream for the CO₂ conversion into DME on the ex-LDH/FER_20 bifunctional catalysts, Figure S6: Catalytic results for CO₂ hydrogenation to DME on ex-LDH/FER_20 bifunctional systems, Figure S7: CO₂ conversion as a function of time on stream for the CO₂ conversion into DME on the CuZnAlZr/FER_20 and CuZnAlZr/ZSM5 bifunctional catalysts, Figure S8: Catalytic results for CO₂ hydrogenation to DME on the CuZnAlZr/FER_20 and CuZnAlZr/ZSM5 bifunctional systems.

Author Contributions: Conceptualization, E.R. and F.F.; methodology, M.M. and L.A.; validation, M.M., S.L., L.A., E.R., F.F. and M.G.C.; formal analysis, M.M., S.L., L.A., E.R., F.F. and M.G.C.; investigation, M.M., S.L., L.A., E.R. and M.G.C.; resources, E.R., F.F., A.P. and M.G.C.; data curation, M.M., S.L., L.A., E.R., F.F. and M.G.C.; writing—original draft preparation, M.M., S.L., L.A., E.R., F.F., A.P. and M.G.C.; writing—review and editing, M.M., S.L., L.A., E.R., F.F., A.P. and M.G.C.; visualization, M.M., S.L., L.A., E.R. and M.G.C.; supervision, E.R., F.F. and A.P.; project administration, E.R. and F.F.; funding acquisition, A.P. All authors have read and agreed to the published version of the manuscript.

Funding: This research was funded by Regione Autonoma della Sardegna, through Sardegna Ricerche, CUP: D49J21001310002, research project “Centre of Excellence on Clean Energy project”.

Conflicts of Interest: The authors declare no conflict of interest. The funders had no role in the design of the study; in the collection, analyses, or interpretation of data; in the writing of the manuscript, or in the decision to publish the results.

References

1. Kim, Y.; Kwon, S.; Song, Y.; Na, K. Catalytic CO₂ hydrogenation using mesoporous bimetallic spinel oxides as active heterogeneous base catalysts with long lifetime. *J. CO₂ Util.* **2020**, *36*, 145–152. [[CrossRef](#)]
2. Bellotti, D.; Sorce, A.; Rivarolo, M.; Magistri, L. Techno-economic analysis for the integration of a power to fuel system with a CCS coal power plant. *J. CO₂ Util.* **2019**, *33*, 262–272. [[CrossRef](#)]
3. Panzone, C.; Philippe, R.; Chappaz, A.; Fongarland, P.; Bengaouer, A. Power-to-Liquid catalytic CO₂ valorization into fuels and chemicals: Focus on the Fisher-Tropsch route. *J. CO₂ Util.* **2020**, *38*, 314–347. [[CrossRef](#)]
4. Sun, Y.; Huang, C.; Chen, L.; Zhang, Y.; Fu, M.; Wu, J.; Ye, D. Active site structure study of Cu/Plate ZnO model catalysts for CO₂ hydrogenation to methanol under the real reaction conditions. *J. CO₂ Util.* **2020**, *37*, 55–64. [[CrossRef](#)]
5. Liu, X.; Cao, C.; Tian, P.; Zhu, M.; Zhang, Y.; Xu, J.; Tian, Y.; Han, Y.F. Resolving CO₂ activation and hydrogenation pathways over iron carbides from DFT investigation. *J. CO₂ Util.* **2020**, *38*, 10–15. [[CrossRef](#)]
6. Youn, M.H.; Park, K.T.; Lee, Y.H.; Kang, S.P.; Lee, S.M.; Kim, S.S.; Kim, Y.E.; Ko, Y.N.; Jeong, S.K.; Lee, W. Carbon dioxide sequestration process for the cement industry. *J. CO₂ Util.* **2019**, *34*, 325–334. [[CrossRef](#)]
7. Runge, P.; Sölch, C.; Albert, J.; Wasserscheid, P.; Zöttl, G.; Grimm, V. Economic comparison of different electric fuels for energy scenarios in 2035. *Appl. Energy* **2019**, *223–224*, 1078–1093. [[CrossRef](#)]
8. Ren, S.; Fan, X.; Shang, Z.; Shoemaker, W.R.; Ma, L.; Wu, T.; Li, S.; Klinghoffer, N.B.; Yu, M.; Liang, X. Enhanced catalytic performance of Zr modified CuO/ZnO/Al₂O₃ catalyst for methanol and DME synthesis via CO₂ hydrogenation. *J. CO₂ Util.* **2020**, *36*, 82–95. [[CrossRef](#)]
9. Jiang, Y.; Yang, H.; Gao, P.; Li, X.; Zhang, J.; Liu, H.; Wang, H.; Wei, W.; Sun, Y. Slurry methanol synthesis from CO₂ hydrogenation over micro-spherical SiO₂ support Cu/ZnO catalysts. *J. CO₂ Util.* **2018**, *26*, 642–651. [[CrossRef](#)]
10. Dang, S.; Yang, H.; Gao, P.; Wang, H.; Li, X.; Wei, W.; Sun, Y. A review of research progress on heterogeneous catalysts for methanol synthesis from carbon dioxide hydrogenation. *Catal. Today* **2019**, *330*, 61–75. [[CrossRef](#)]
11. Guil-López, R.; Mota, N.; Llorente, J.; Millán, E.; Pawelec, B.; Fierro, J.L.G.; Navarro, R.M. Methanol Synthesis from CO₂: A Review of the Latest Developments in Heterogeneous Catalysis. *Materials* **2019**, *12*, 3902. [[CrossRef](#)]
12. Li, K.; Chen, J.G. CO₂ Hydrogenation to Methanol over ZrO₂-Containing Catalysts: Insights into ZrO₂ Induced Synergy. *ACS Catal.* **2019**, *9*, 7840–7861. [[CrossRef](#)]
13. Kourtelesis, M.; Kousi, K.; Kondarides, D.I. CO₂ Hydrogenation to Methanol over La₂O₃-Promoted CuO/ZnO/Al₂O₃ Catalysts: A Kinetic and Mechanistic Study. *Catalysts* **2020**, *10*, 183. [[CrossRef](#)]
14. Mota, N.; Millán Ordoñez, E.; Pawelwc, B.; Fierro, J.L.G.; Navarro, R.M. Direct Synthesis of Dimethyl Ether from CO₂: Recent Advances in Bifunctional/Hybrid Catalytic Systems. *Catalysts* **2021**, *11*, 411. [[CrossRef](#)]
15. Gao, W.; Wang, H.; Wang, Y.; Guo, W.; Jia, M. Dimethyl ether synthesis from CO₂ hydrogenation on La-modified CuO-ZnO-Al₂O₃/HZSM-5 bifunctional catalysts. *J. Rare Earths* **2013**, *31*, 470–476. [[CrossRef](#)]
16. Bonura, G.; Cordaro, M.; Cannilla, C.; Mezzapica, A.; Spadaro, L.; Arena, F.; Frusteri, F. Catalytic behaviour of a bifunctional system for the one step synthesis of DME by CO₂ hydrogenation. *Catal. Today* **2014**, *228*, 51–57. [[CrossRef](#)]
17. Montesano, R.; Narvaez, A.; Chadwick, D. Shape-selectivity effects in syngas-to-dimethyl ether conversion over Cu/ZnO/Al₂O₃ and zeolite mixtures: Carbon deposition and by-product formation. *Appl. Catal. A Gen.* **2014**, *482*, 69–77. [[CrossRef](#)]
18. Frusteri, F.; Bonura, G.; Cannilla, C.; Drago Ferrante, G.; Aloise, A.; Catizzzone, E.; Migliori, M.; Giordano, G. Stepwise tuning of metal-oxide and acid sites of CuZnZr-MFI hybrid catalysts for the direct DME synthesis by CO₂ hydrogenation. *Appl. Catal. B Environ.* **2015**, *176–177*, 522–531. [[CrossRef](#)]
19. Frusteri, F.; Migliori, M.; Cannilla, C.; Frusteri, L.; Catizzzone, E.; Aloise, A.; Giordano, G.; Bonura, G. Direct CO₂-to-DME hydrogen reaction: New evidences of a superior behaviour of FER-based hybrid systems to obtain high DME. *J. CO₂ Util.* **2017**, *18*, 353–361. [[CrossRef](#)]
20. Catizzzone, E.; Aloise, A.; Migliori, M.; Giordano, G. From 1-D to 3-D zeolite structures: Performance assessment in catalysis of vapour-phase methanol dehydration to DME. *Micropor. Mesopor. Mater.* **2017**, *243*, 102–111. [[CrossRef](#)]
21. Ren, S.; Shoemaker, W.R.; Wang, X.; Shang, Z.; Klinghoffer, N.; Li, S.; Yu, M.; He, X.; White, T.A.; Liang, X. Highly active and selective Cu-ZnO based catalyst for methanol and dimethyl ether synthesis via CO₂ hydrogenation. *Fuel* **2019**, *239*, 1125–1133. [[CrossRef](#)]
22. Ren, S.; Li, S.; Klinghoffer, N.; Yu, M.; Liang, X. Effects of mixing methods of bifunctional catalysts on catalyst stability of DME synthesis via CO₂ hydrogenation. *Carbon Resour. Convers.* **2019**, *2*, 85–94. [[CrossRef](#)]
23. Bonura, G.; Cannilla, C.; Frusteri, L.; Mezzapica, A.; Frusteri, F. DME production by CO₂ hydrogenation: Key factors affecting the behaviour of CuZnZr/ferrierite catalysts. *Catal. Today* **2017**, *281*, 337–344. [[CrossRef](#)]
24. Sheng, Q.; Ye, R.-P.; Gong, W.; Shi, X.; Xu, B.; Argyle, M.; Adidharma, H.; Fan, M. Mechanism and catalytic performance for direct dimethyl ether synthesis by CO₂ hydrogenation over CuZnZr/ferrierite hybrid catalyst. *J. Environ. Sci.* **2020**, *92*, 106–117. [[CrossRef](#)] [[PubMed](#)]

25. Song, F.; Tan, Y.; Xie, H.; Zhang, Q.; Han, Y. Direct synthesis of dimethyl ether from biomass-derived syngas over Cu-ZnO-Al₂O₃-ZrO₂(x)/γ-Al₂O₃ bifunctional catalysts: Effect of Zr-loading. *Fuel Process. Technol.* **2014**, *126*, 88–94. [[CrossRef](#)]
26. Suwannapichat, Y.; Numpilai, T.; Chanlek, N.; Faungnawakij, K.; Chareonpanich, M.; Limtrakul, J.; Witoon, T. Direct synthesis of dimethyl ether from CO₂ hydrogenation over novel hybrid catalysts containing a Cu-ZnO-ZrO₂ catalyst admixed with WO_x/Al₂O₃ catalysts: Effects of pore size of Al₂O₃ support and W loading content. *Energy Convers. Manag.* **2018**, *159*, 20–29. [[CrossRef](#)]
27. Muhamad, E.N.; Irmawati, R.; Tautiq-Yap, Y.H.; Abdullah, A.H.; Kniep, B.L.; Girgsdies, F.; Ressler, T. Comparative study of Cu/ZnO catalysts derived from different precursors as a function of aging. *Catal. Today* **2008**, *131*, 118–124. [[CrossRef](#)]
28. Baltes, C.; Vukojevic, S.; Schuth, F. Correlations between synthesis, precursor, and catalyst structure and activity of a large set of CuO/ZnO/Al₂O₃ catalysts for methanol synthesis. *J. Catal.* **2008**, *258*, 334–344. [[CrossRef](#)]
29. Zhang, Q.; Zuo, Y.Z.; Han, M.H.; Wang, J.F.; Jin, Y.; Wei, F. Long carbon nanotubes intercrossed Cu/Zn/Al/Zr catalyst for CO/CO₂ hydrogenation to methanol/dimethyl ether. *Catal. Today* **2010**, *150*, 55–60. [[CrossRef](#)]
30. Gao, P.; Li, F.; Xiao, F.; Zhao, N.; Sun, N.; Wei, W.; Zhong, L.; Sun, Y. Preparation and activity of Cu/Zn/Al/Zr catalysts via hydrotalcite-containing precursors for methanol synthesis from CO₂ hydrogenation. *Catal. Sci. Technol.* **2012**, *2*, 1447–1454. [[CrossRef](#)]
31. Frusteri, L.; Cannilla, C.; Todaro, S.; Frusteri, F.; Bonura, G. Tailoring of Hydrotalcite-Derived Cu-Based Catalysts for CO₂ Hydrogenation to Methanol. *Catalysts* **2019**, *9*, 1058. [[CrossRef](#)]
32. Kühl, S.; Schumann, J.; Kasatkin, I.; Havecker, M.; Schlögl, R.; Behrens, M. Ternary and quaternary Cr or Ga-containing ex-LDH catalysts—Influence of the additional oxides onto the microstructure and activity of Cu/ZnAl₂O₄ catalysts. *Catal. Today* **2015**, *246*, 92–100. [[CrossRef](#)]
33. Behrens, M.; Kasatkin, I.; Kühl, S.; Weinberg, G. Phase-Pure Cu,Zn,Al Hydrotalcite-like Materials as Precursors for Copper rich Cu/ZnO/Al₂O₃ Catalysts. *Chem. Mater.* **2010**, *22*, 386–397. [[CrossRef](#)]
34. Rouquerol, F.; Rouquerol, J.; Sing, K.S.W.; Llewellyn, P.; Maurin, G. *Adsorption by Powders and Porous Solids: Principles, Methodology and Applications*, 2nd ed.; Academic Press-Elsevier: Amsterdam, The Netherlands, 2014; pp. 12–13.
35. Guo, X.; Mao, D.; Wang, S.; Wu, G.; Lu, G. Combustion synthesis of CuO-ZnO-ZrO₂ catalysts for the hydrogenation of carbon dioxide to methanol. *Catal. Commun.* **2009**, *10*, 1661–1664. [[CrossRef](#)]
36. Jang, J.; Kim, G.-P.; Chang, T.-S.; Kim, B.-S.; Shim, S.F.; Park, S.H.; Baek, S.-H. Preparation of Nanostructured CuO/ZnO/Al₂O₃ Catalysts for the Synthesis of Methanol from Syngas. *J. Nanosci. Nanotechnol.* **2016**, *16*, 10887–10891. [[CrossRef](#)]
37. Gao, P.; Li, F.; Zhan, H.; Zhao, N.; Xiao, F.; Wei, W.; Zhong, L.; Sun, Y. Fluorine-modified Cu/Zn/Al/Zr catalysts via hydrotalcite-like precursors for CO₂ hydrogenation to methanol. *Catal. Commun.* **2014**, *50*, 78–82. [[CrossRef](#)]
38. Gao, P.; Xie, R.; Wang, H.; Zhong, L.; Xia, L.; Zhang, Z.; Wei, W.; Sun, Y. Cu/Zn/Al/Zr catalysts via phase-pure hydrotalcite-like compounds for methanol synthesis from carbon dioxide. *J. CO₂ Util.* **2015**, *11*, 41–48. [[CrossRef](#)]
39. Xiao, S.; Zhang, Y.; Gao, P.; Zhong, L.; Li, X.; Zhang, Z.; Wang, H.; Wei, W.; Sun, Y. Highly efficient Cu-based catalysts via hydrotalcite-like precursors for CO₂ hydrogenation to methanol. *Catal. Today* **2017**, *281*, 327–336. [[CrossRef](#)]
40. Jung, K.-D.; Joo, O.-S.; Han, S.-H. Structural change of Cu/ZnO by reduction of ZnO in Cu/ZnO with methanol. *Catal. Lett.* **2000**, *68*, 49–54. [[CrossRef](#)]
41. Hajduk, Š.; Dasireddy, V.D.B.C.; Likozar, B.; Dražić, G.; Orel, Z.C. CO_x-free hydrogen production via decomposition of ammonia over Cu-Zn-based heterogeneous catalysts and their activity/stability. *Appl. Catal. B Environ.* **2017**, *211*, 57–67. [[CrossRef](#)]
42. Atzori, L.; Rombi, E.; Meloni, D.; Monaci, R.; Sini, M.F.; Cutrufello, M.G. Nanostructured Ni/CeO₂-ZrO₂ catalysts for CO₂ conversion into SNG. *J. Nanosci. Nanotechnol.* **2019**, *19*, 3269–3276. [[CrossRef](#)] [[PubMed](#)]
43. Atzori, L.; Cutrufello, M.G.; Meloni, D.; Cannas, C.; Gazzolli, D.; Monaci, R.; Sini, M.F.; Rombi, E. Highly active NiO-CeO₂ catalysts for synthetic natural gas production by CO₂ methanation. *Catal. Today* **2018**, *299*, 183–192. [[CrossRef](#)]
44. Li, C.; Yuan, X.; Fujimoto, K. Development of highly stable catalyst for methanol synthesis from carbon dioxide. *Appl. Catal. A Gen.* **2014**, *469*, 306–311. [[CrossRef](#)]
45. Bonura, G.; Arena, F.; Mezzatesta, G.; Cannilla, C.; Spadaro, L.; Frusteri, F. Role of the ceria promoter and carrier on the functionality of Cu-based catalysts in the CO₂-to-methanol hydrogenation reaction. *Catal. Today* **2011**, *171*, 251–256. [[CrossRef](#)]
46. Angelo, L.; Kobl, K.; Martinez Tejada, L.M.; Zimmermann, Y.; Parkhomenko, K.; Roger, A.-C. Study of CuZnMO_x oxides (M = Al, Zr, Ce, CeZr) for the catalytic hydrogenation of CO₂ into methanol. *C. R. Chim.* **2015**, *18*, 250–260. [[CrossRef](#)]
47. Gao, P.; Li, F.; Zhao, N.; Xiao, F.; Wei, W.; Zhong, L.; Sun, Y. Influence of modifier (Mn, La, Ce, Zr and Y) on the performance of Cu/Zn/Al catalysts via hydrotalcite-like precursors for CO₂ hydrogenation to methanol. *Appl. Catal. A Gen.* **2013**, *468*, 442–452. [[CrossRef](#)]
48. Shi, Z.; Tan, Q.; Wu, D. Ternary copper-cerium-zirconium mixed metal oxide catalyst for direct CO₂ hydrogenation to methanol. *Mater. Chem. Phys.* **2018**, *219*, 263–272. [[CrossRef](#)]
49. Wang, W.; Qu, Z.; Song, L.; Fu, Q. An investigation of Zr/Ce ratio influencing the catalytic performance of CuO/Ce_{1-x}Zr_xO₂ catalyst for CO₂ hydrogenation to CH₃OH. *J. Energy Chem.* **2020**, *47*, 18–28. [[CrossRef](#)]
50. García-Trenco, A.; Martínez, A. Direct synthesis of DME from syngas on hybrid CuZnAl/ZSM-5 catalysts: New insights into the role of zeolite acidity. *Appl. Catal. A Gen.* **2012**, *411–412*, 170–179. [[CrossRef](#)]
51. Bonura, G.; Cordaro, M.; Spadaro, L.; Cannilla, C.; Arena, F.; Frusteri, F. Hybrid Cu-ZnO-ZrO₂/H-ZSM5 system for the direct synthesis of DME by CO₂ hydrogenation. *Appl. Catal. B Environ.* **2013**, *140–141*, 16–24. [[CrossRef](#)]

52. Okuhara, T. Water-Tolerant Solid Acid Catalysts. *Chem. Rev.* **2002**, *102*, 3641–3666. [[CrossRef](#)] [[PubMed](#)]
53. Cavani, F.; Trifirò, F.; Vaccari, A. Hydrotalcite-type anionic clays: Preparation, properties and applications. *Catal. Today* **1991**, *11*, 173–301. [[CrossRef](#)]
54. Klug, H.P.; Alexander, L.E. *X-ray Diffraction Procedures: For Polycrystalline and Amorphous Materials*, 2nd ed.; Wiley & Sons Inc.: New York, NY, USA, 1974; pp. 687–703.
55. Gervasini, A.; Bennici, S. Dispersion and surface states of copper catalysts by temperature-programmed-reduction of oxidized surfaces (s-TPR). *Appl. Catal. A Gen.* **2005**, *281*, 199–205. [[CrossRef](#)]
56. Pettinau, A.; Mureddu, M.; Ferrara, F. Carbon Dioxide Conversion into Liquid Fuels by Hydrogenation and Photoelectrochemical Reduction: Project Description and Preliminary Experimental Results. *Energy Procedia* **2017**, *114*, 6893–6904. [[CrossRef](#)]
57. Mureddu, M.; Ferrara, F.; Pettinau, A. Highly efficient CuO/ZnO/ZrO₂@SBA-15 nanocatalysts for methanol synthesis from the catalytic hydrogenation of CO₂. *Appl. Catal. B Environ.* **2019**, *258*, 117941. [[CrossRef](#)]